Andrzej Zieliński*, Anita Cymann, Adrian Gumiński, Anna Hernik and Grzegorz Gajowiec

Influence of High Temperature Oxidation on Hydrogen Absorption and Degradation of Zircaloy-2 and Zr 700 Alloys

https://doi.org/10.1515/htmp-2017-0074
Received May 23, 2017; accepted July 30, 2017

Abstract: The present research was aimed at determining the effects of the oxide layers on hydrogen absorption, microstructure and mechanical properties of the Zircaloy-2 and Zr 702 alloys. The oxidation was made at 350 °C, 700 °C and 900 °C for 10 to 30 min in laboratory air, followed by hydrogen cathodic charging for 72 h and annealing at 400 °C for 4 h. The slow strain rate tests were carried out on oxidized, charged and annealed specimens. The oxidation resulted in thick and cracked, more for Zr 702 alloy, layer. After oxidation at 350 °C, the appearance of hydrides in Zircaloy-2 and absence of hydrides in Zr 702 alloy were observed. After oxidation at high temperatures no current flow was noticed at applied voltage up to 5 V, and no hydrogen or hydrogen cracks. The observed effects were attributed to the phase structure of investigated alloys at low hydrogen content.

Keywords: zirconium alloys, oxidation, hydrogen degradation

Introduction

Some Zr alloys are used in nuclear industry as fuel claddings [1–3], reflectors for light water reactors [4] and in spent nuclear fuel reprocessing plants [5, 6]. The Zr alloys possess high corrosion resistance at usual operating conditions, but during nuclear accidents, like a loss-of-coolant accident (LOCA), they are simultaneously exposed to oxygen and hydrogen. Such exposure of fuel claddings may result in their rapid oxidation, descaling of oxide layers, hydrogen absorption and material degradation [1, 7].

***Corresponding author: Andrzej Zieliński,** Department of Materials Engineering and Bonding, The Gdansk University of Technology, Narutowicza 11/12, 80-233 Gdansk, Poland,
E-mail: azielins@pg.gda.pl
Anita Cymann, Adrian Gumiński, Anna Hernik, Grzegorz Gajowiec, Department of Materials Engineering and Bonding, The Gdansk University of Technology, Narutowicza 11/12, 80-233 Gdansk, Poland

The oxides forming a surface layer may appear in three forms: as monoclinic ZrO_2 at low and middle temperatures, tetragonal phase stable between 1170 °C and 2370 °C (1443–2643 K), and cubic structure above the extreme temperature [8]. The original nanometric oxide films composed of two zones, the porous outer and dense and defective inner zone [9]. The oxide layers are microcrystalline and grow into columnar grains [7]. The beginning of thermodynamic transformations, kinetics of oxide formation and properties of different oxide layers depend significantly on material structure and environment. The monoclinic ZrO_2 phase of few hundred nanometers thick was predominant at 200 °C in Zircaloy-4 [9], and in research on few other Zr alloys, the evolution of both monoclinic and tetragonal phases was observed between 350 °C and 1050 °C in some environments [8].

The rapid oxidation at high temperatures may result in thick and cracked oxide layers. They may undergo to so-called breakaway oxidation: descaling of the oxide layers from the substrate arising from their cracking. The source of cracking is the appearance of thermal stresses caused by different volume expansion coefficients of substrate and oxide phase or two oxide phases, or oxide porosity [2–11]. The start of breakaway oxidation depends on temperature, an environment, and material composition. The breakaway oxidation in the range of 950–1200 °C was observed, depending on the alloy, to start in time from 12 ks to 2 ks [10]. In another research in nitrogen-free steam, the breakaway was found at 1027 °C [11] after 5.5 ks of exposure.

Atomic hydrogen, which is formed as an effect of water decomposition during the LOCA, appears in zirconium alloys in interstitial solution, as hydrogen bonded by crystal defects, particularly dislocations and interfaces, and as hydrides. The terminal hydrogen solubility in zirconium is about 80 mass ppm at 300 °C and 200 mass ppm at 400 °C [2]. Two stable hydride phases, δ-hydride (fcc) and ε-hydride (fct), and one metastable phase, γ-hydride (fct), were distinguished, depending on the temperature and hydrogen content [12].

The zirconium alloys may be either strengthened or softened by hydrogen, based on hydrogen content and

temperature [13]. The softening is due to interstitial hydrogen solution and appears at low hydrogen content resulting in the decrease in Young's modulus, shear modulus and microhardness [13, 14], and an entirely ductile fracture [15, 16]. The presence of hydrides at higher hydrogen content usually manifested in often slightly increased (sometimes decreased) room tensile strength, decreased ductility and elongation [17–21]. The brittle behavior of the zirconium alloy was observed already at 220 ppm [22]. The cleavage facets were found on the fracture surfaces of pure zirconium and a mixture of dimples and cleavage facets for the Zr-Nb alloys [23].

The present research was aimed at investigating the barrier effect of oxide layers formed at different temperature against the hydrogen entry. Two alloys of different microstructure were chosen, the two-phase Zircaloy-2 used for fuel claddings and single phase Zr 702 alloy; the different microstructure of both alloys may affect both formations of oxide layers and hydrogen absorption, diffusion, and susceptibility to hydrogen-enhanced degradation.

Experimental

The Zircaloy-2 and Zr 702 alloy were investigated, their composition shown in Table 1. The first alloy has two phase microstructure composed of Zr matrix with dispersed $Zr(Fe, Cr)_2$ precipitates. The second alloy has a single phase, a solid solution of Hf in Zr.

Table 1: The chemical composition of tested materials (according to standards).

Alloy	Content, wt. pct.					
	Hf	Sn	Cr	Fe	Ni	Zr
Zircaloy-2	–	1.2–1.7	0.05–0.15	0.07–0.20	0.03–0.08	rem.
Zr 702	≤ 4.5	–	≤ 0.05	–		rem.

The smooth specimens were cut from the rods in a direction transverse to the rolling direction. The specimens had dimensions 120 mm of total length, 50 mm of the duration of working part and 4 mm of diameter. The specimens were polished with abrasive papers, No. 2000 as the last, and diamond paste of 3 μm of granulation, and then cleaned in distilled water in an ultrasonic bath and dried in warm air.

Afterward, the specimens were put in the electric oven and heated for 10, 20 or 30 min. in laboratory air. The heating temperature was maintained at 350 °C, 700 °C or 900 °C. The first temperature corresponds to the usual working conditions of zirconium claddings; the others approach the conditions of the LOCA. The specimens were put in the oven already heated to the high temperatures, and after the oxidation, they were removed from the oven.

Then the specimens were electrolytically charged with hydrogen. This method allows obtaining relatively small amounts of hydrogen when comparing to the gaseous charging. The cathodic charging was performed at room temperature at voltage 2.6 V. The specimen was a cathode, and Pt counter electrode was an anode. After charging the samples were removed from the solution, cleaned with distilled water, dried in warm air and annealed for 4 h at 400 °C to obtain the uniform distribution of hydrogen inside the entire specimen.

The annealed samples were subjected to the slow strain rate test (SSRT) at 10^{-6} s^{-1} strain speed in laboratory air. The force and elongation were monitored during the tensile tests. When using the SSRTs, one might expect the highest interaction between hydrogen and mechanical stress.

The microscopic examinations of the specimens were performed with the JEOL 7800 F scanning electron microscope on the cross-sections of polished specimens before any test (reference samples), after the oxidation and after the hydrogen charging. The etching of cross-sections was made with the solution containing 45 cm^3 of 65 % HNO_3, 10 cm^3 of 40 % HF and 45 cm^3 of distilled water. After tension, similar examinations were performed on fracture faces to determine the presence and distribution of hydrides, and the mechanism and path of failure.

The hydrogen content was measured by the LECO method at the Silesian University of Technology.

Results

Oxidation effects

For both alloys, the oxidation at 350 °C led to the oxide layer of few nanometers thick.

For the Zircaloy-2 oxidized at 700 °C, the oxide layers were compact without visible cracks. The layers were porous and inhomogeneous. The oxidation at 900 °C, even after 10 min., resulted in the numerous transverse (circumferential) and single longitudinal cracks passing through the whole oxide layer. After 20 min many groups

of such cracks were observed. The width of the cracks sometimes achieved 1 μm. The thickness of the oxide layer was the largest near the cracks. The pile-ups of cracks resulted in descaling of the oxides.

The examinations of cross-sections of this alloy showed the increasing thickness of the oxide layer from 3.5 μm after 10 min through 5 μm after 20 min and about 6 μm after 30 min of oxidation at 700 °C. The cracks penetrating the substrate were exceptionally observed. After the oxidation at 900 °C, the thickness of the oxide layer was 15–17 μm for all oxidation times. In this case, the cracks appeared on the surface after 20 min of oxidation and were relatively long, even to 35 μm. The oxide layer was substantially thicker in this area. The oxide grains formed the elongated columnar structures. The small submicron pores appeared between the grains. The surfaces and cross-sections obtained after oxidation at 900 °C of the Zircaloy-2 are shown in Figure 1.

The oxidation had essentially different behavior for the Zr 702 alloy. The oxides did not form any tight layer after oxidation at 700 °C, and the cracks appeared already after 10 min. Longer branched cracks were observed after oxidation at 900 °C. The descaling appeared 10 min of oxidation, and after 20 min the surface was highly broken. Two zones of oxides, inner and outer, were found. After 30 min of oxidation, the crevices were seen with naked eye.

The examinations of cross-sections of this alloy showed no uniform oxide layer, due to descaling even at oxidation at 700 °C. The layer thickness was higher than for the Zircaloy-2 alloy. The surfaces and cross-sections obtained after oxidation at 900 °C of the Zr 702 alloy are shown in Figure 2.

Hydrogen charging effects

The applied voltage resulted in the current density 80 mA/cm^2 for specimens oxidized at 350 °C and in total blocking of current flow for 3 days for samples oxidized at higher temperatures (even if the voltage was increased to 5 V). The strong hydrogen barrier effect of oxide layers of 20 μm around the hydrides was already postulated [24]. The hydrogen amount ranged between 30 and 80 mass ppm.

Figure 3 shows the cross-sections for both materials, either only oxidized at 350 °C or oxidized, hydrogen charged and annealed. For Zircaloy-2 alloy, many hydride long lines were observed after oxidation. For Zr 702 alloy no hydrides were found.

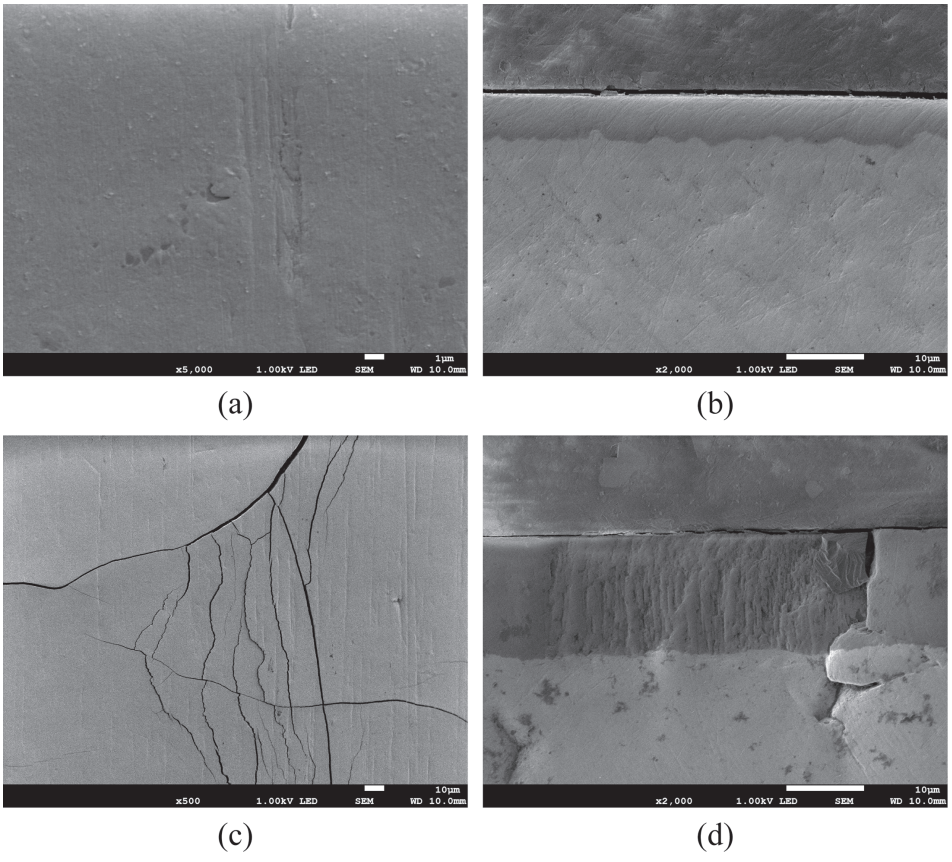

Figure 1: The surfaces (a, c) and cross-sections (b, d) of the Zircaloy-2 alloy oxidized at 700 °C (a, b) and 900 °C (c, d) for 30 min.

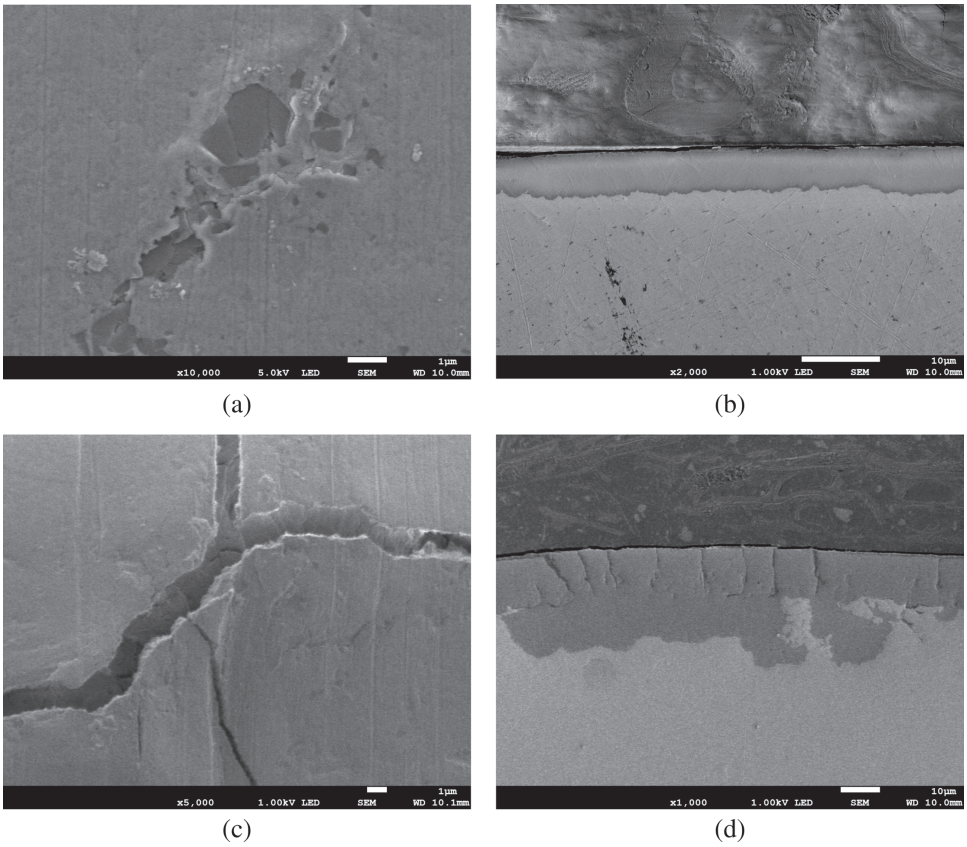

Figure 2: The surfaces (a, c) and cross-sections (b, d) of the Zr 702 alloy oxidized at 700 °C (a, b) and 900 °C (c, d) for 30 min.

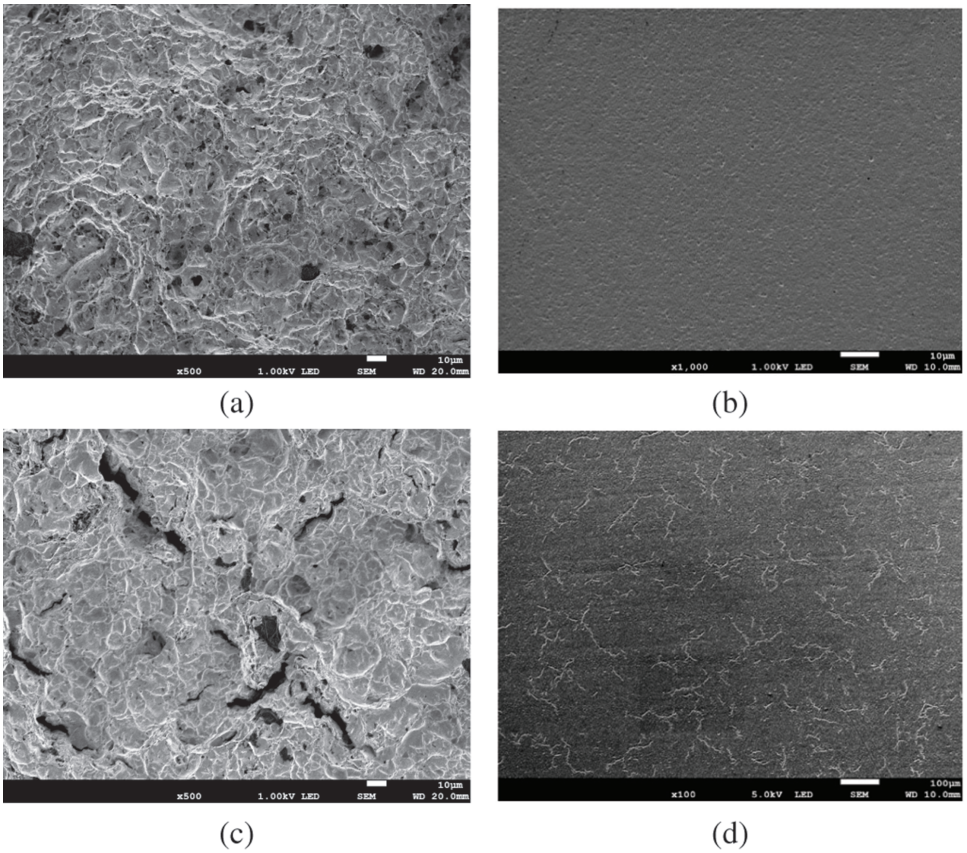

Figure 3: The cross-sections (a, c) and fracture faces (b, d) for the Zircaloy-2 alloy subjected to slow strain rate test: reference specimen (a, b) and after oxidization at 350 °C for 30 min, hydrogen charging and annealing (c, d).

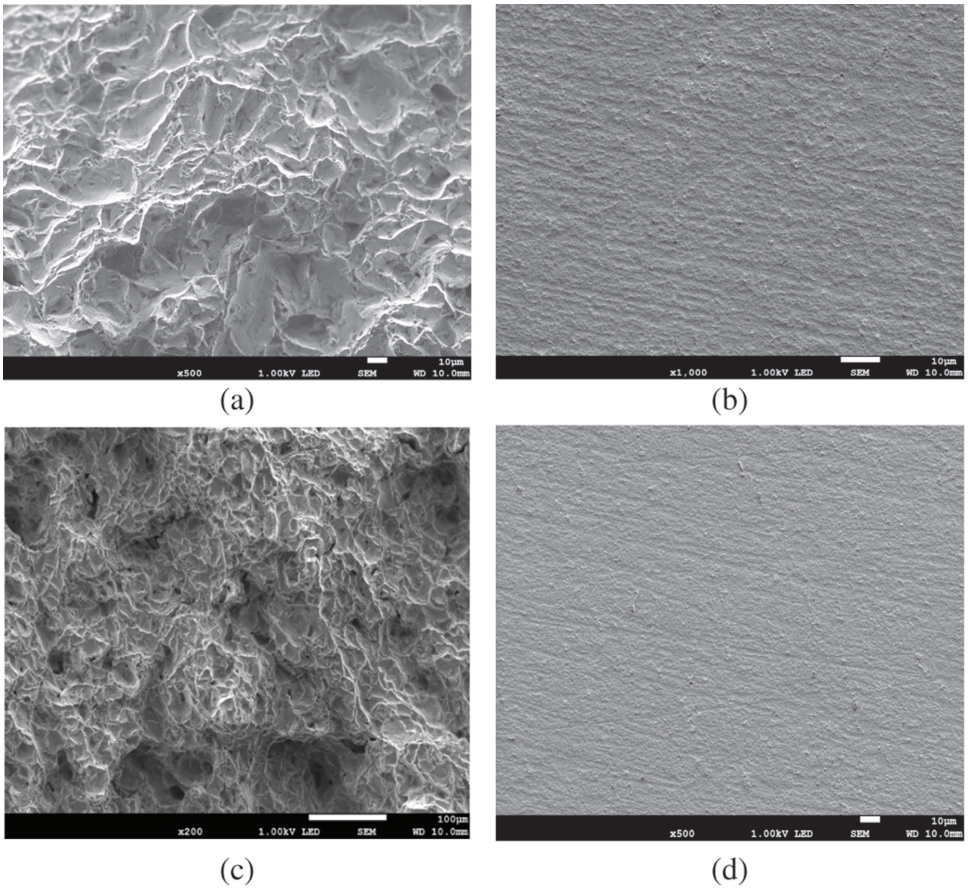

Figure 4: The cross-sections (a, c) and fracture faces (b, d) for the Zr 702 alloy subjected to slow strain rate test: reference specimen (a, b) and after oxidization at 350 °C for 30 min, hydrogen charging and annealing (c, d).

Figure 4 demonstrates the fracture faces of both materials, either only oxidized at 350 °C or oxidized, hydrogen charged and annealed. The intercrystalline crack paths with many dimples and totally ductile fracture were observed for both alloys. The brittle behavior was noticed only near the cracks.

Table 2 shows the values of tensile strength and elongation for both materials, either only oxidized at 350 °C or oxidized, hydrogen charged and annealed. Hydrogen presence slightly increased the elongation of the tested alloys and had no effect on the tensile strength within the limits of experimental error.

Table 2: The tensile strength and elongation for no charged and hydrogen charged alloys, as measured in slow strain rate tests.

Alloy	Treatment	Tensile strength UTS ± SD MPa	Elongation ε ± SD %
Zr 702	Oxidized at 350 °C	366.32 ± 5.73	25.79 ± 0.54
	Oxidized at 350 °C, hydrogen charged and annealed	360.92 ± 6.97	27.25 ± 1.28
Zircaloy-2	Oxidized at 350 °C	516.64 ± 16.30	21.42 ± 0.84
	Oxidized at 350 °C, hydrogen charged and annealed	518.23 ± 13.14	23.69 ± 1.67

Discussion

Oxidation effects

The oxidation time in the range of 10–30 min has a particular influence on layer thickness as predicted by kinetic laws. The cracks also develop with the oxidation time as related to the oxygen diffusion. The above phenomena are dependent on the oxidation temperature, which affects the number, length, and width of cracks appearing inside the oxide layers. The effects of both oxidation temperature and time on the appearance of oxide layers on zirconium and its alloys were already extensively investigated [25]. What is new, it is an occurrence of degradation of oxide layers at 700 °C, being an evidence of an important role of thermal stresses in the initiation of cracking, likely in the area of triple grain

boundaries. The experiments were designed to obtain such stresses after oxidation and removal of specimens from the oven to air. It means that in LOCA conditions, the formed oxide layers would always be cracked.

On the other hand, the effect of chemical composition on this behavior is undeniable and significant. There is few data on the oxidation of Zr 702 alloy [26]. It is known that unalloyed zirconium forms white porous oxide films, and zircaloys – dark tightly adherent oxide layer. The Zr 702 alloy is a single phase alloy, in which zirconium and hafnium dissolve entirely each other. Therefore this alloy has relatively low mechanical properties and the less protective oxide layer. For that reason, the cracking and descaling process start are more developed for the Zr 702 alloy than for the Zircaloy-2.

In all previous research and this one, thin oxide layers of as-received or working in normal conditions Zr alloys were demonstrated. Such layers cannot show any barrier effect against hydrogen. In past research, the mobile hydrogen absorption followed by metal degradation was attributed to the breakaway effect and direct hydrogen absorption by a bare metal. Such effect is important: when oxides are removed, are highly porous or cracked, the possibility for hydrogen to enter the metal might be similar to that of the as-received alloy. The observed no current flow for specimens oxidized at 700 °C and 900 °C show that even in the presence of such deteriorated surface the layer is still able actually to retard the hydrogen entry.

The microscopic examinations of surface layers for Zr alloys oxidized at high temperature may give an evidence of the layer condition and start of breakaway oxidation. The measurements of current flow performed here for cathodically charged alloys allow establishing whether the barrier effect is still present or begin to disappear after high temperature oxidation. Both phenomena are unnecessarily associated with each other likely because – as we prove here – the cracks do not contribute to a great extent to the hydrogen passage from the oxide surface into bare metal. The different chemical and phase contents for both Zr alloys affect the oxidation and oxide degradation process, but they have no direct influence on susceptibility to hydrogen deterioration, at least assessed by an appearance or lack of hydrides.

Hydrogen effects

This research shows the essential difference in behavior of two tested alloys about hydrogen behavior in the alloy. The Zircaloy-2 alloy demonstrates the appearance of hydrides after oxidation at 350 °C but not after oxidation at a higher temperature. On the contrary, the Zr 702 alloy reveals no hydrides after oxidation at any temperature. The mechanism of hydrogen degradation in zirconium and its alloys may be described by successive stages: (i) discharge of hydrogen ions on the metal surface in sulfuric acid, followed by either (ii) their recombination or (iii) entry of atomic hydrogen into zirconium, (iv) diffusion of hydrogen through the metal retarded by its (v) trapping by some precipitates and dislocations, (vi) hydrogen repartition between mobile hydrogen in interstitial solution, (vii) hydrogen bonding by weak and vigorous traps, and (viii) hydrides' formation, if hydrogen amount in two previous forms exceeds terminal solubility. The resistance of the last alloy to hydrogen-enhanced degradation may be assumed as resulting from the effects of chemical and phase composition on either hydrogen absorption, diffusion or hydrides' formation.

The hydrogen absorption is strictly related to the thickness and continuity of the oxide layer. The oxides grown on the Zr alloys are more permeable for deuterium than those on pure zirconium because of a greater number of grains and grain boundaries, and different their chemistry [27, 28]. The susceptibility of oxidized Zr alloys to hydrogen pick-up was suggested to be determined by conductivity in the inner part of the barrier layer, which could enable reduction of hydrogen ingress, shifting the location of cathodic half-cell reaction away from the metal [29]. However, after oxidation at 350 °C, the layers of both alloys are thin, and hydrogen absorption is easy.

Another possible effect of chemical composition on total hydrogen pick-up fraction (ratio of absorbed hydrogen to the overall generating hydrogen) cannot also explain the lack of hydrides in the Zr 702 alloy. The entire pick-up portion is lower for the Zr-Sn alloy than for pure zirconium, the last possessing structure similar to the Zr 702 alloy [30]. Thus, the hydrogen absorption should be higher for the Zr 702 alloy, and an absence of hydrides cannot be explained by different amounts of entering hydrogen.

The differences in bulk diffusion between both alloys are also negligible as zirconium forms a matrix in both materials. The presence of precipitates may retard the diffusion in the Zircaloy-2 alloy as they form strong hydrogen traps. The applied cathodic charging has been already used several times [8, 15, 16, 18, 20] and may result in hydrogenation of Zr alloys even at slow hydrogen diffusion at room temperature; hydrogen may migrate within thin oxide film into bare metal, and subsequent annealing makes its concentration profile across

the sample very uniform. Summarizing, the differences in chemical and phase contents between both investigated alloys have no significant effect on hydrogen absorption and diffusion.

The absence of hydrides for the Zr 702 alloy may be then attributed only to the alloy structure. In the Zircaloy-2 alloy, the entering hydrogen is easily bounded by precipitates $Zr(Fe, Cr)_2$ [26], here observed. The local high hydrogen content exceeds its terminal solubility, and the hydrides may appear, grow and decompose at such sites [7]. In the Zr 702 alloy, with no precipitates encountered according to phase diagram and some tests [14], all hydrogen is, after annealing at 400 °C for 4 h, in solid solution. After fast cooling, either oversaturated hydrogen solid solution or submicronic hydrides may form. The different phase composition and presence or lack of precipitates are then the only valuable explanation of observed behavior.

The proposed model is supported by the results of mechanical tests. Hydrogen did not here affect the mechanical strength, within the limits of experimental error. The small increase in ductility may be attributed to the effect of solid hydrogen solution. The brittle behavior was found only near the cracks in the matrix. Such complex localized expression was observed not only in Zr alloys, but also in Ni-based metals [31]. That means that at the small amount of hydrogen, being here below 100 ppm and a little above the limit hydrogen solubility in zirconium, the number of hydrides is insufficient to cause the macroscopically brittle behavior of both alloys; for the Zr 702 single phase alloy such phenomenon could be observed only at much higher hydrogen content. The observed results support the hydrogen-enhanced localized plasticity (HELP) degradation model in dilute H solution and hydrogen-enhanced decohesion (HEDE) in concentrated H solution [32]. The appearance of each mechanism depends, according to our results, also on an alloy and its microstructure: for single phase alloys the HELP model is applicable, and for two-phase alloys with precipitates dispersed in the matrix, the HEDE mechanism becomes prevalent close to the interfaces hydride – matrix. The first mechanism is associated with the plastic flow, the second – with cleavage cracking.

Conclusions

The Zr 702 alloy is more prone than Zircaloy-2 to surface cracking at high temperature, presumably because of a lack of alloying elements strengthening the oxide layer.

The oxide layers, formed on surfaces of both Zircaloy-2 and Zr 702 alloys oxidized at 700 °C and 900 °C, constitute very effective barriers against hydrogen entry, in spite of surface cracking.

The high resistance to hydrogen-enhanced degradation of the Zr 702 alloy, manifesting in the absence of hydrides in bulk, can be explained by a lack of phase precipitates serving as potential sites of hydride nucleation.

The small increase in plasticity of both alloys may be an evidence of their softening, supporting the dislocation mechanism of hydrogen-enhanced degradation at hydrogen contents below 100 ppm.

Acknowledgments: The authors wish to thank Prof. Waldemar Serbinski for his helpful comments. The research was supported by the Polish National Science Center under the project entitled “Hydrogen degradation of oxidized zirconium alloys,” No. 2013/11/B/ST8/04328.

References

[1] A. Zielinski and S. Sobieszczyk, Intl. J. Hydrogen Energy, 36 (2011) 8619–8629.
[2] T.R. Allen, R.J.M. Konings and A.T. Motta, Corrosion of Zirconium Alloys, [in] Comprehensive Nuclear Materials edited by R.J.M. Konings, Elsevier, Amsterdam, Vol. 5 (2012), pp. 49–68.
[3] C. Yan, R. Wang, Y. Wang, X. Wang and G. Bai, Nucl. Eng. Techn., 47 (2015) 323–331.
[4] M. Nader and A. Mohamed, Nucl. Sci. Eng., 173 (2013) 172–181.
[5] U. Kamachi Mudali, A. Ravi Shankar, R. Natarajan, N. Saibaba and B. Raj, Nucl. Techn., 182 (2013) 349–357.
[6] J. Jayaraj, K. Thyagarajan, C. Mallika and U. Kamachi Mudali, Nucl. Techn., 191 (2015) 58–70.
[7] M. Steinbrück and M. Böttcher, J. Nucl. Mater., 414 (2011) 276–285.
[8] N. Selmi and A. Sari, Adv. Mater. Phys. Chem., 3 (2013) 168–173.
[9] C. Zeng, Y. Ling, Y. Bai, R. Zhang, X. Dai and Y. Chen, Intl. J. Hydrogen Energy, 41 (2016) 7676–7690.
[10] J.H. Baek and Y.H. Jeong, J. Nucl. Mater., 372 (2008) 152–159.
[11] J. Birchley and L. Fernandez-Moguel, Ann. Nucl. Energy, 40 (2012) 163–170.
[12] L. Lanzani and M. Ruch, J. Nucl. Mater., 324 (2004) 165–176.
[13] M. Le Saux, J. Besson, S. Carassou, C. Poussard and X. Averty, Eng. Fail. Analys., 17 (2010) 683–700.
[14] S. Yamanaka, D. Setoyama, H. Muta, M. Uno, M. Kuroda, K. Takeda and T. Matsuda, J. Alloys Comp., 372 (2004) 129–135.
[15] G. Bertolino, G. Meyer and J. Perez Ipiña, J. Alloys Comp., 330-332 (2002) 408–413.
[16] G. Bertolino, G. Meyer and J. Perez Ipiña, J. Nucl. Mater., 320 (2003) 272–279.

[17] M.S. Blackmur, J.D. Robson, M. Preuss, O. Zanellato, R.J. Cernik, S.-O. Shi, F. Ribeiro and J. Andrieux, J. Nucl. Mater., 464 (2015) 160–169.
[18] S.I. Hong, K.W. Lee and K.T. Kim, J. Nucl. Mater., 303 (2002) 169–176.
[19] J.H. Kim, M.H. Lee, B.K. Choi and Y.H. Jeong, J. .Alloys Comp., 431 (2007) 155–161.
[20] K.W. Lee and S.I. Hong, J. Alloys Comp., 346 (2002) 302–307.
[21] S.-J. Min, M.-S. Kim and K.-T. Kim, J. Nucl. Mater., 441 (2013) 306–314.
[22] J.-H. Huang and M.-S. Yeh, Met. Mater. Trans. A, 29 (1998) 1047–1056.
[23] S. Oh, C. Jang, J.H. Kim and Y.H. Jeong, Mater. Sci. Eng., 527 (2010) 1306–1313.
[24] W. Chen, L. Wang and L. Shigang, J. Alloys Compd., 469 (2009) 142–145.
[25] P.A. Schweitzer, Fundamentals of Metallic Corrosion: Atmospheric and Media Corrosion of Metals, Chpt. 22: Zirconium, CRC Press (2006), pp. 581–582.
[26] K.M. McHugh, J.E. Garnier, S. Rashkeev, M.V. Glazoff, G.W. Griffith and S.M. Bragg-Sitton, High Temperature Steam Corrosion of Cladding for Nuclear Applications: Experimental, [in] Ceramic Materials for Energy Applications III, edited by Hua-Tay Lin, Yutai Katoh, Alberto Vomiero, Soshu Kirihara, Sujanto Widjaja, The Amer. Ceram. Soc Wiley Online Library., (2014), pp. 149–160.
[27] G. Sundell, M. Thuvander and H.-O. Andren, Corr. Sci., 102 (2016) 490–502.
[28] M.B. Elmoselhi, J. Alloys Compd., 231 (1995) 716–721.
[29] A. Couet, A.T. Motta and R.J. Comstock, J. Nucl. Mater., 451 (2014) 1–13.
[30] M. Große, E. Lehmann, M. Steinbrück, G. Kühne and J. Stuckert, J. Nucl. Mater., 385 (2009) 339–345.
[31] J. Blach and L. Falat, High Temp. Mater. Proc., 33 (2014) 329–337.
[32] P. Chakraborty, A. Moitra and T. Saha-Dasgupta, J. Nucl. Mater., 466 (2015) 172–178.